Water Absorption and Hygrothermal Aging Study on Organomontmorillonite Reinforced Polyamide 6/Polypropylene Nanocomposites

W. S. Chow, A. Abu Bakar, Z. A. Mohd Ishak

School of Materials and Mineral Resources Engineering, Engineering Campus, Universiti Sains Malaysia, Seri Ampangan 14300 Nibong Tebal, Penang, Malaysia

Received 2 July 2004; accepted 22 February 2005
DOI 10.1002/app.22172
Published online in Wiley InterScience (www.interscience.wiley.com).

ABSTRACT: The water absorption and hygrothermal aging behavior of organomontmorillonite (OMMT) reinforced polyamide 6/polypropylene (PA6/PP ratio = 70/30), with and without maleated PP (MAH-*g*-PP), was studied at three different temperatures (30, 60, and 90°C). The water absorption and hygrothermal aging response of the composites was studied and analyzed by tensile tests and morphology assessment (scanning electron microscopy and transmission electron microscopy), indicating the effect of the immersion temperature, OMMT, and MAH-*g*-PP compatibilizer. The mathematical treatment used in analyzing the data was the single free phase model of diffusion, which assumed Fickian diffusion and utilized Fick's second law of diffusion. The kinetics of water absorption of the PA6/PP nanocomposites conformed to Fickian law behavior, whereby the initial moisture absorption follows a linear relationship between the percentage gain at any time t and $t^{1/2}$ (the square root of time), followed by saturation. It was found that the equilibrium moisture content and the diffusion coefficient are dependent on the OMMT loading, MAH-*g*-PP concentration, and immersion temperatures. Both the tensile modulus and strength of the PA6/PP nanocomposites deteriorated after being exposed to hygrothermal aging. MAH-*g*-PP acted as a good compatibilizer for PA6/PP/OMMT nanocomposites, which was attributed to its higher retention ability in modulus and strength (in the wet and redried states), lower equilibrium moisture content, and reduced water diffusivity of the nanocomposites. Morphological sketches for both uncompatibilized and MAH-*g*-PP compatibilized PA6/PP/OMMT nanocomposites, toward water uptake are proposed.
 J Appl Polym Sci 98: 780–790, 2005

Key words: polyamide 6/polypropylene nanocomposites; organoclay; water absorption; hygrothermal aging

INTRODUCTION

Hygrothermal aging is a degradation process that combines the effects of moisture and temperature and results in substantial deterioration of the mechanical properties. According to Mohd Ishak and Berry,[1] the moisture penetration (i.e., diffusion) mechanism becomes active only after the occurrence of specific damage to the composites, which is exposure of the composite to a hot and moist environment. Numerous researchers described investigations of hygrothermal aging on nylon 6/6,[1] poly(butylene terephthalate),[2–4] poly(ethylene terephthalate),[5] polypropylene (PP),[6] epoxy,[7–10] bismaleimide,[11,12] vinylester,[13] and polyimide.[14,15] However, there is still very limited publication on the hygrothermal aging of nanocomposites.

This article reports on the water absorption and hygrothermal aging of a polyamide 6 (PA6)/PP nanocomposite in the presence of organomontmorillonite (OMMT) and maleated PP (MAH-*g*-PP). Focus is also be given to determining the effect of hygrothermal aging on the tensile behavior and morphology of both uncompatibilized and MAH-*g*-PP compatibilized PA6/PP/OMMT nanocomposites. In spite of processing to give good mechanical properties, PA6 shows poor resistance to water and moisture, which is attributed to the presence of amide groups in PA6. A minor portion of a hydrophobic component (30 wt % PP) was added into the PA6 matrix to improve the water resistance of PA6.

Naturally occurring MMT is incompatible with most polymers because of its hydrophilic nature. Thus, ion exchange is widely practiced to modify the MMT surface to increase its compatibility with mostly hydrophobic materials. However, it is believe that OMMT still has a tendency to absorb moisture, which can be traced to the functional group (intercalant) in the silicate clay. In our previous work on PA6/PP nanocomposites, 4 phr OMMT was observed to be the optimum loading for the blends, and it was estab-

Correspondence to: Z. A. Mohd Ishak (zarifin@eng.usm.my).

Contract grant sponsor: Ministry of Science, Technology and Environment, Malaysia; contract grant number: 063171/IRPA.

TABLE I
Designation of Materials

Designation	Composition	Parts
PA6/PP	PA6/PP	70/30
PA6/PP/2TC	PA6/PP/organomontmorillonite	70/30/2
PA6/PP/4TC	PA6/PP/organomontmorillonite	70/30/4
PA6/PP/6TC	PA6/PP/organomontmorillonite	70/30/6
PA6/PP/8TC	PA6/PP/organomontmorillonite	70/30/8
PA6/PP/10TC	PA6/PP/organomontmorillonite	70/30/10
PA6/PP/5M/4TC	PA6/PP/MAHgPP/organomontmorillonite	70/30/5/4
PA6/PP/10M/4TC	PA6/PP/MAHgPP/organomontmorillonite	70/30/10/4

lished that the OMMT is well dispersed (intercalated and exfoliated) and preferentially embedded in the PA6 phase.[16] A significant improvement in the strength and stiffness of the composites was reported when MAH-*g*-PP was used as a compatibilizer for the PA6/PP blend. The MAH-*g*-PP compatibilized blend based nanocomposites showed a more homogeneous morphology and better clay dispersion than the uncompatibilized counterparts.[17]

This study attempts to enhance the water resistance and mechanical performance of PA6/PP by using OMMT (acting as reinforcing agent and impermeable silicate layers) and MAH-*g*-PP (acting as compatiblizer to improve the interfacial bonding between PA6 and PP). Investigation of hygrothermal aging of the composites is carried out through study of the kinetics of moisture absorption. Thus, it is the aim of the present contribution to report on the effect of OMMT and MAH-*g*-PP on the water absorption and hygrothermal aging behavior of a PA6/PP nanocomposite at three immersion temperatures (30, 60, and 90°C).

EXPERIMENTAL

Specimen preparation

Melt compounding of the PA6/PP (70/30) blends and nanocomposites was done on a counterrotating twin-screw extruder (Berstoff). The extrusion zone temperature ranged from 220 to 230°C. Prior to extrusion, PA6 pellets and OMMT were dehumidified by using a vacuum oven at 80°C for 8 h. The extrudates were pelletized with a Haake pelletizer. The pellets were injection molded into standard tensile bars using a Niigata AN 50 injection-molding machine. The injection-molding temperature ranged from 225 to 240°C. Prior to injection molding, all pellets were dehumidified in a vacuum oven at 80°C for 8 h. The tensile test specimens were molded in a type I mold according to ASTM D-638. The designations of the materials are presented in Table I.

Water absorption and hygrothermal aging test

Specimens (tensile bars) were dried at 80°C in a vacuum oven until a constant weight was attained. Then they were immersed in hot water in a thermostated stainless steel water bath at 30, 60, and 90°C. Weight gains were recorded by periodic removal of the specimens from the water bath and weighing on a balance with a precision of 1 mg. The percentage gain at any time t (M_t) as a result of moisture absorption was determined by eq. (1):

$$M_t\ (\%) = (W_w - W_d)/W_d \times 100 \qquad (1)$$

where W_d and W_w denote the weight of dry material (the initial weight of materials prior to exposure to the hygrothermal aging) and weight of materials after exposure to hygrothermal aging, respectively. The percentage equilibrium, or maximum moisture absorption (M_m), was calculated as an average value of several consecutive measurements that showed no appreciable additional absorption. The weight gain, resulting from moisture absorption, can be expressed in terms of two parameters, the diffusion coefficient or diffusivity (D) and the M_m, using the following equation:

$$\frac{M_t}{M_m} = 1 - \frac{8}{\pi^2} exp\left[-\left(\frac{Dt}{h^2}\right)\pi^2 \right] \qquad (2)$$

where h is the thickness of the sample.

Mechanical properties

Tensile tests were performed on a 5582 tensile testing machine at 23°C, according to ASTM D-638, at a crosshead speed of 50 mm/min. The tensile modulus, tensile strength, and elongation at break were evaluated from the stress–strain data.

Microscopy examination

The fracture surface of selected PA6/PP based nanocomposites was inspected using a scanning electron microscopy (SEM) microscope (model S 360, Leica Cambridge Ltd.). SEM micrographs were taken with 10-kV acceleration voltage at various magnifications. Prior to the SEM examinations, the fractured parts of the specimens were mounted on aluminum stubs and

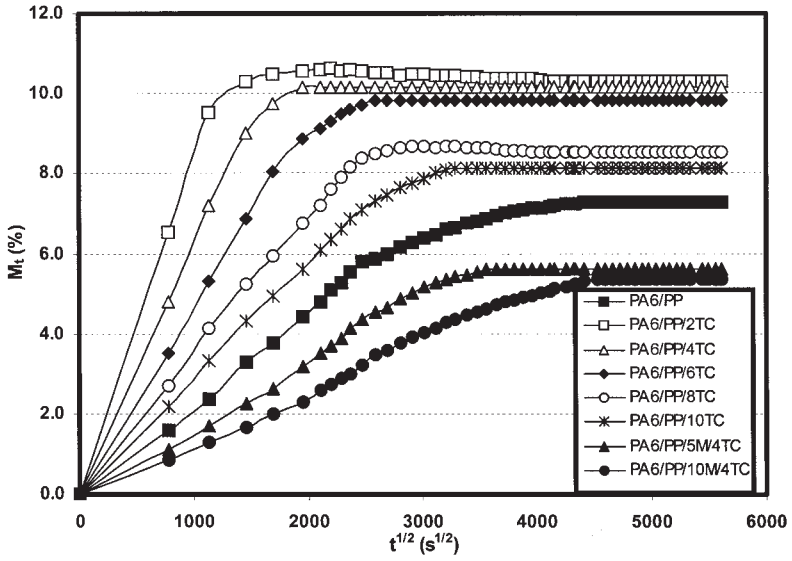

(a)

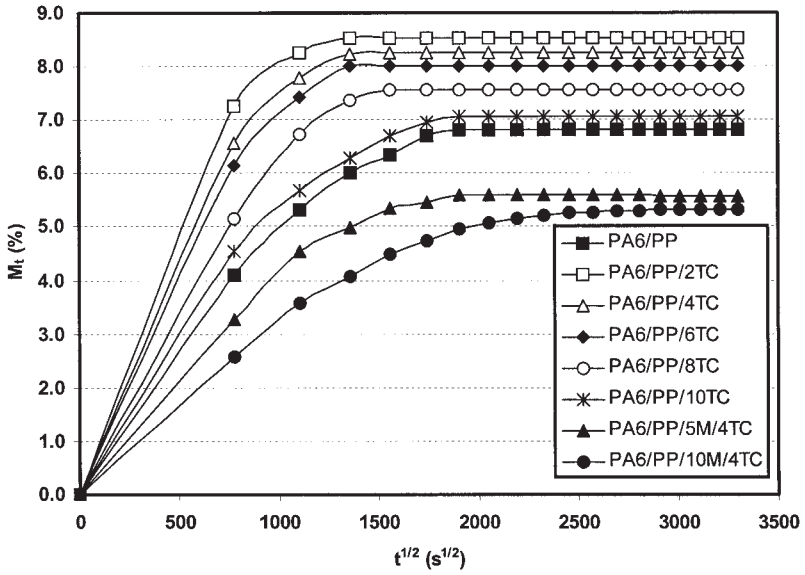

(b)

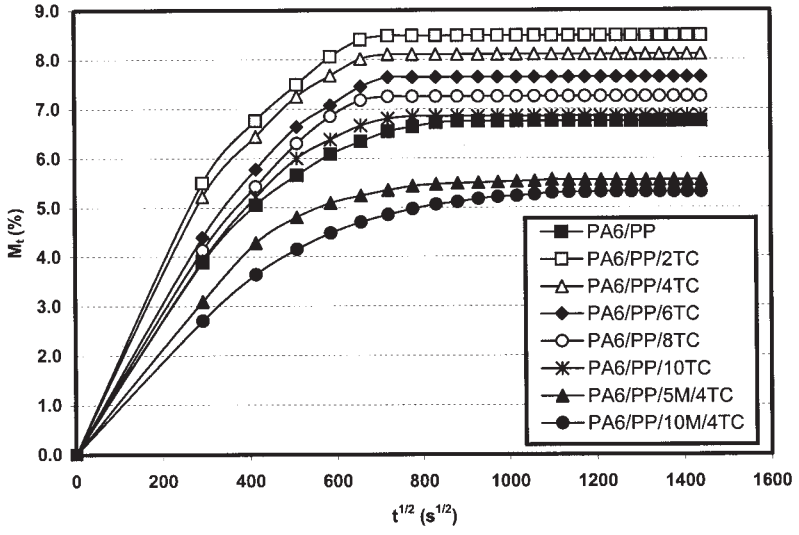

(c)

Figure 1 The effect of organoclay loading and compatibilizer (MAH-*g*-PP) on the moisture uptake of PA6/PP blends during (a) water absorption at 30°C, (b) hygrothermal aging at 60°C, and (c) hygrothermal aging at 90°C.

TABLE II
Effect of Immersion Temperature on Diffusivity (D) and Equilibrium Moisture Content (M_m) of PA6/PP/Organomontmorillonite Nanocomposites

	Immersion temperature					
	30°C		60°C		90°C	
Material	M_m (%)	D ($\times 10^{-10}$ m^2/s)	M_m (%)	D ($\times 10^{-10}$ m^2/s)	M_m (%)	D ($\times 10^{-10}$ m^2/s)
PA6/PP	7.28	0.9	6.82	1.7	6.75	11.0
PA6/PP/2TC	10.30	3.2	8.53	3.4	8.48	13.9
PA6/PP/4TC	10.17	2.7	8.25	2.9	8.10	13.7
PA6/PP/6TC	9.84	1.9	8.01	2.7	7.64	10.9
PA6/PP/8TC	8.52	1.2	7.57	2.2	7.25	10.8
PA6/PP/10TC	8.14	0.8	7.07	1.9	6.85	10.7
PA6/PP/5M/4TC	5.60	0.5	5.60	1.6	5.55	10.2
PA6/PP/10M/4TC	5.37	0.3	5.34	1.1	5.31	8.59

sputter coated with a thin layer of gold to avoid electrostatic charging during examination. Transmission electron microscopy (TEM) measurements were carried out with a LEO 912 Omega transmission electron microscope applying an acceleration voltage of 120 keV. The specimens were prepared by using an Ultracut E (Reichert and Jung) ultramicrotome. Thin sections (about 100-nm thickness) were cut with a Diatome diamond knife at room temperature.

RESULTS AND DISCUSSION

Kinetics of moisture absorption

Figure 1(a–c) shows the percentage moisture absorption (M_t) of PA6/PP/OMMT as a function of $t^{1/2}$ at immersion temperatures of 30, 60, and 90°C. An initial linear relationship between M_t and $t^{1/2}$ was observed in each case, followed by saturation. This indicates

Figure 2 A TEM picture showing the dispersion of the organoclay in the PA6 matrix.

TABLE III
Tensile Properties of PA6/PP Nanocomposites in AR, HA, and RD States

			Immersion temperature					
			30°C		60°C		90°C	
Material	Mechanical properties	Control	Wet	Redried	Wet	Redried	Wet	Redried
PA6/PP	Tensile modulus (GPa)	1.9	1.7 (89.5)	1.8 [94.7]	1.5 (80.7)	1.7 [89.5]	0.5 (26.3)	1.3 [68.4]
	Tensile strength (MPa)	32.1	28.7 (89.4)	29.4 [91.6]	26.3 (81.8)	27.1 [84.4]	22.8 (71.0)	24.6 [76.6]
	Elongation at break (%)	22.8	20.2 (88.6)	21.3 [93.4]	18.4 (80.6)	19.6 [86.0]	10.2 (44.7)	14.6 [64.0]
PA6/PP/2TC	Tensile modulus (GPa)	1.9	1.7 (89.5)	1.8 [94.7]	1.5 (80.7)	1.7 [89.5]	0.6 (31.6)	1.3 [68.4]
	Tensile strength (MPa)	36.4	31.2 (85.7)	32.7 [89.9]	21.9 (60.1)	26.5 [72.7]	20.4 (56.0)	23.3 [64.0]
	Elongation at break (%)	14.9	15.5 (104.0)	14.8 [99.3]	15.8 (106.0)	14.9 [99.9]	17.5 (117.4)	14.7 [98.7]
PA6/PP/4TC	Tensile modulus (GPa)	2.1	1.8 (85.7)	1.9 [90.5]	1.6 (76.3)	1.9 [90.5]	0.7 (33.3)	1.5 [71.4]
	Tensile strength (MPa)	38.0	27.3 (71.8)	30.8 [81.1]	20.7 (54.5)	24.8 [62.3]	18.5 (48.6)	24.8 [65.3]
	Elongation at break (%)	4.2	5.6 (133.3)	4.0 [95.2]	6.4 (152.3)	4.2 [99.8]	7.8 (185.7)	4.1 [97.6]
PA6/PP/6TC	Tensile modulus (GPa)	2.2	1.9 (86.4)	2.0 [90.9]	1.7 (75.9)	2.0 [90.9]	0.8 (36.4)	1.6 [72.7]
	Tensile strength (MPa)	36.4	27.6 (75.8)	29.8 [81.8]	19.9 (54.5)	23.2 [63.6]	17.0 (46.7)	22.7 [62.4]
	Elongation at break (%)	2.6	3.6 (138.5)	2.5 [96.1]	4.6 (176.9)	2.5 [96.2]	4.8 (184.6)	2.5 [96.2]
PA6/PP/8TC	Tensile modulus (GPa)	2.3	2.0 (86.9)	2.1 [91.3]	1.8 (75.4)	2.0 [86.9]	0.9 (39.1)	1.7 [73.9]
	Tensile strength (MPa)	31.0	26.8 (86.5)	27.3 [88.0]	17.5 (56.2)	24.3 [78.4]	14.8 (47.7)	20.1 [64.8]
	Elongation at break (%)	1.9	2.6 (136.8)	1.8 [94.7]	3.2 (168.4)	1.8 [94.7]	3.6 (189.5)	1.8 [94.7]
PA6/PP/10TC	Tensile modulus (GPa)	2.4	2.1 (87.5)	2.2 [91.7]	1.9 (78.2)	2.1 [87.5]	0.9 (37.5)	1.8 [75.0]
	Tensile strength (MPa)	29.2	20.7 (70.9)	24.2 [82.8]	16.2 (55.6)	22.1 [75.6]	13.7 (46.9)	19.4 [66.4]
	Elongation at break (%)	1.5	1.9 (126.7)	1.4 [93.3]	2.4 (157.9)	1.4 [93.3]	2.8 (186.7)	1.4 [93.3]
PA6/PP/5M/4TC	Tensile modulus (GPa)	2.4	2.2 (91.6)	2.3 [95.8]	2.1 (88.2)	2.2 [91.6]	1.3 (54.2)	2.0 [83.3]
	Tensile strength (MPa)	49.7	45.5 (91.5)	47.8 [96.2]	42.7 (85.9)	44.2 [88.9]	28.4 (57.1)	41.6 [83.7]
	Elongation at break (%)	4.8	7.2 (150.0)	4.7 [97.9]	7.8 (162.8)	4.7 [97.9]	10.8 (225.0)	4.7 [97.9]
PA6/PP/10M/4TC	Tensile modulus (GPa)	2.3	2.1 (91.3)	2.2 [95.6]	2.0 (86.9)	2.1 [91.3]	1.2 (52.2)	1.9 [82.6]
	Tensile strength (MPa)	48.5	45.4 (93.6)	46.2 [95.3]	43.0 (88.8)	45.1 [93.1]	29.5 (60.8)	40.9 [84.3]
	Elongation at break (%)	5.3	8.4 (158.5)	5.2 [98.1]	9.4 (187.7)	5.2 [98.1]	12.3 (232.0)	5.2 [98.1]

The values in parentheses are the percentage retention of the tensile properties after hygrothermal aging, and the values in brackets are the percentage recovery of the tensile properties after redrying.

that Fickian behavior was observed. The M_m and D values are summarized in Table II.

It is interesting to note that both M_m and D values of the PA6/PP/OMMT nanocomposite are higher than those of neat PA6/PP blends. This is contrary to the data reported for microcomposites such as short carbon fiber reinforced PA6[1] and short glass fiber reinforced poly(butylene terephthalate).[3] In microcomposites, the presence of short fibers has been reported to reduce both M_m and D values. The opposite trend, which was observed in the present study, indicates that the nature of the interaction between the water molecules with the OMMT filled nanocomposites is very much different than its interaction with short glass fibers and/or short carbon fibers. The higher M_m and D values may be attributed to the hydrophilic nature of octadecylamine groups, which act as an intercalant in the OMMT. It is known that the OMMT used in this study contained about 30 wt % octadecylamine intercalant.[16,17] Thus, when the silicate layers are exfoliated/intercalated, some of the intercalant group in the OMMT will be available for interaction with the water molecules. It is believed that there is a strong possibility for the intercalant to interact with water molecules, forming hydrogen bonding.

Another possible reason is that water molecules can penetrate and intercalate into the gallery of the layered silicate of OMMT, and subsequently increase the diffusion rate. However, increasing the OMMT decreased both M_m and D values. This may be attributed to the possibility of agglomeration of clay at a higher loading of OMMT, which could hinder moisture penetration into the nanocomposites. This is supported by the evidence obtained from TEM analysis that is presented later (Fig. 2). There is also a possibility that the poor interfacial bonding between PA6/PP and OMMT may also influence the nature of the moisture uptake. In the fiber reinforced composites, for instance, interfacial damage was observed to be one of the main factors responsible for the enhancement of moisture penetration into the composites.[3] It is suggested that, in addition to diffusion, the OMMT (in platelike and high aspect ratio) may give rise to other mechanisms of moisture absorption, such as capillarity, transport by microcracks, and water interaction with the intercalant (octadecylamine) in the OMMT.

From Table II it can be seen that both M_m and D values are reduced remarkably in the presence of MAH-*g*-PP. Both values are even lower than that of the neat PA6/PP blends. This provides a clear indication that the resistance to moisture uptake has been enhanced via compatibilization. The amide–amine reaction that occurred between the MAH groups of the

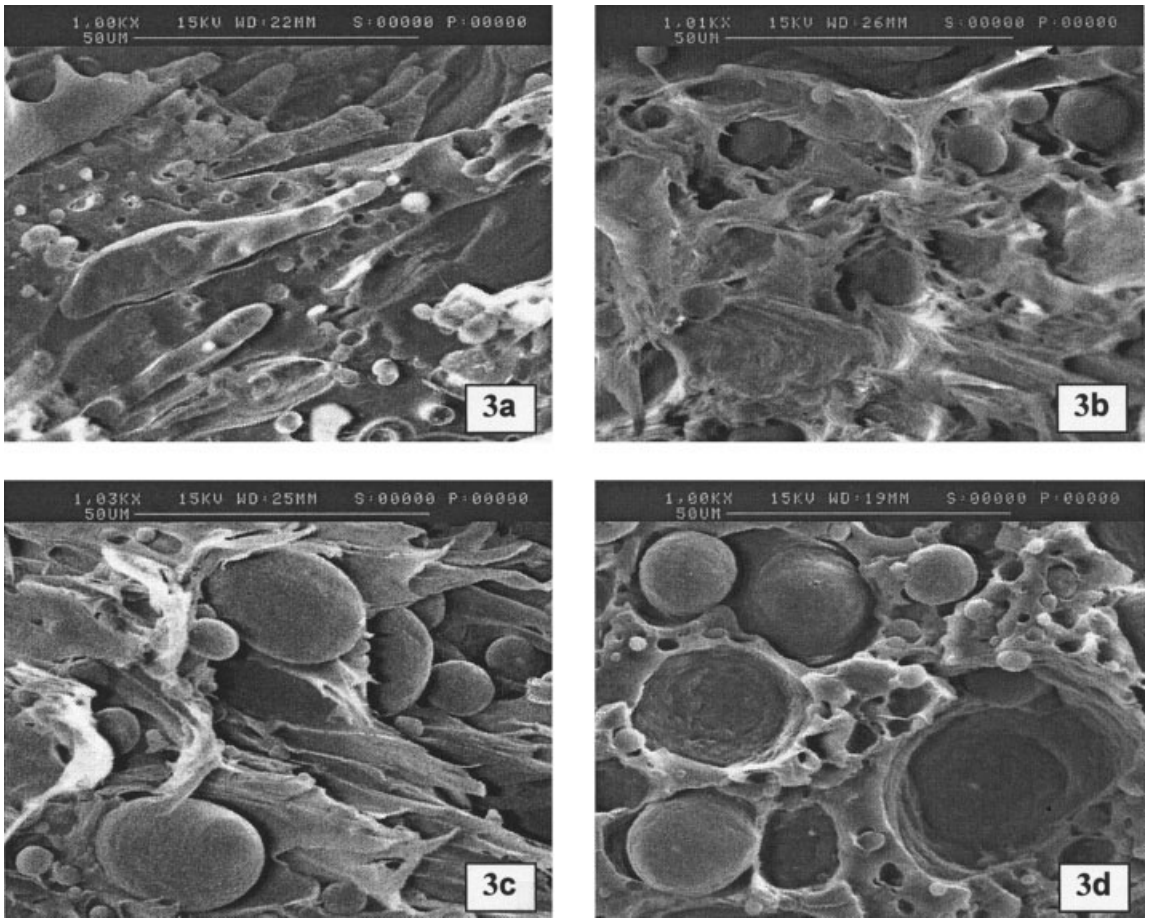

Figure 3 SEM micrographs taken of (a) control and (b–d) the tensile fractured surface of PA6/PP blends after being subjected to hygrothermal aging at (b) 30, (c) 60, and (d) 90°C.

compatibilizer and octadecylamine groups of the clay is believed to have resulted in a significant improvement of the interfacial adhesion between PA6, PP, and OMMT, and subsequently reduced the diffusion rate. The amide–amine reaction reduces the chances for the water molecules to interact with octadecylamine intercalant groups in the OMMT, as in the case of uncompatibilized PA6/PP/OMMT. The effect of MAH-*g*-PP compatibilization is also clearly manifested in the mechanical performance of the nanocomposites upon subjecting to hygrothermal aging. The possible chemical interaction between PA6, PP, OMMT, and MAH-*g*-PP was proposed earlier by Chow et al.[17]

Mechanical properties

Table III shows the tensile properties of the PA6/PP blend and its nanocomposites in as-received, hygrothermal aging, and redried states. The effect of OMMT loading on the tensile properties of PA6/PP has been discussed earlier.[16] From Table III, it can be seen that both the tensile strength and tensile modulus of OMMT reinforced PA6/PP decreased after being subjected to hygrothermal aging. The low percentage of retention ability in the tensile strength indicates that hygrothermal aging has caused a dramatic reduction in the strength of the nanocomposites. This may arise as a result of the combined effect of plasticization of the PA6 phase in the PA6/PP matrix (as evidenced by the increase in the elongation at break of the composites in the wet states), as well as the degradation of the polymer–OMMT interface. Upon redrying, the strength of the nanocomposites is almost fully recovered, as in the case of neat PA6/PP. The differences in the percentage recovery between PA6/PP and its nanocomposites lie in the fact that, in the latter, the action of water may have resulted in the partial disruption of the bonds between the OMMT and PA6/PP matrix and the formation of additional microcavities, which will be filled with water. Upon drying, these cavities will act as stress concentrators, which can then initiate matrix cracking, leading to reductions in both the stiffness and strength of the composites. According to Mohd Ishak and Berry,[1] as the water conditioning temperature increases, the moisture attack on the interface becomes more significant. Thus, at higher

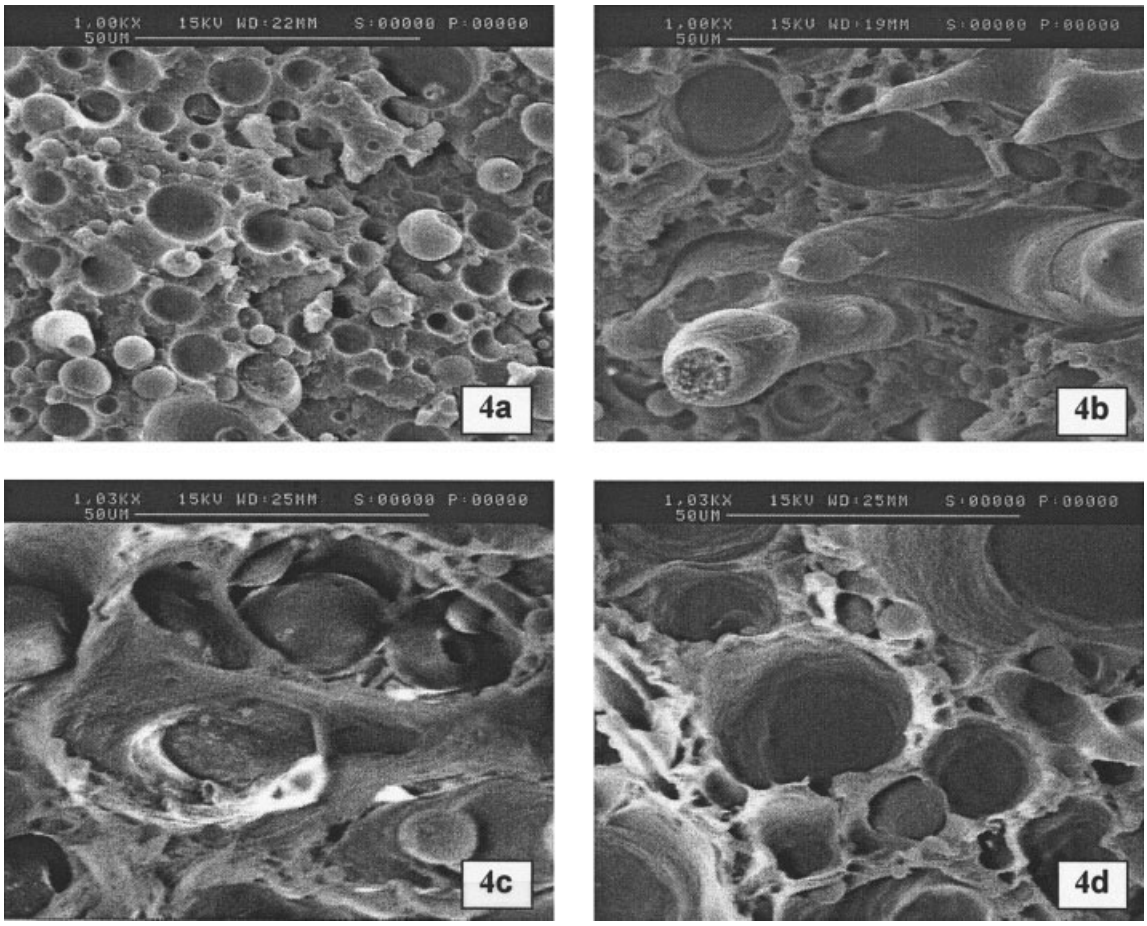

Figure 4 SEM micrographs taken of (a) control and (b–d) the tensile fractured surface of PA6/PP/OMMT nanocomposites after being subjected to hygrothermal aging at (b) 30, (c) 60, and (d) 90°C.

temperatures, the efficiency of stress transfer decreases and an overall reduction in strength and stiffness is observed.

Note that the incorporation of MAH-*g*-PP compatibilizer into PA6/PP nanocomposites has increased the retention ability of the composites when subjected to hygrothermal aging (Table III). For hygrothermal aging at 90°C, the percentage retention of tensile strength is slightly higher (almost 61%) compared to only about 48% for the uncompatibilized nanocomposites. Upon redrying, the percentage recovery of as high as 84% of the tensile strength has been recorded for the PA6/PP nanocomposites compatibilized with MAH-*g*-PP. This indicates that the interaction of the water molecules with the PA6/PP matrix is physical in nature, and water is merely acting as a plasticizer. The excellent recoverability of MAH-*g*-PP compatibilized PA6/PP/OMMT may be attributed to the improvement of interfacial adhesion between PA6 and PP by the addition of MAH-*g*-PP.

It is interesting to note that the elongation at break of the PA6/PP blend decreased with increasing immersion temperatures. In contrast, the elongation at break of both uncompatibilized and compatibilized PA6/PP/OMMT showed an opposite trend: it increases as the immersion temperature increases. In the former, the moisture uptake behavior can be explained in terms of the moisture-induced plasticization of PA6 and the incompatibility between PA6 and PP. As the immersion temperature increases, the rate of diffusion of water into the PA6/PP samples will increase. As the PA6 became softened because of the plasticization effect of the water molecules, the "poor interface" between the PA6 and PP will be further weakened. This will consequently limit the extent of plastic deformation of the PA6 surrounding the PP particles (in the form of shear yielding). As for PA6/PP/OMMT, the moisture uptake behavior can be explained in terms of a few phenomena, including moisture-induced plasticization of PA6, partially hygroscopic behavior of OMMT, and "moisture-induced microcavitation" of OMMT. Recall that OMMT possesses a unique combination of characteristics (viz., rigidity, platelike, high aspect ratio, good thermal stability), is partially hygroscopic, and has an exfoliation/intercalation feature. Accordingly, the OMMT, and its silicate layers when exfoliated, are aligned in the mold flow direction during injection molding.[16]

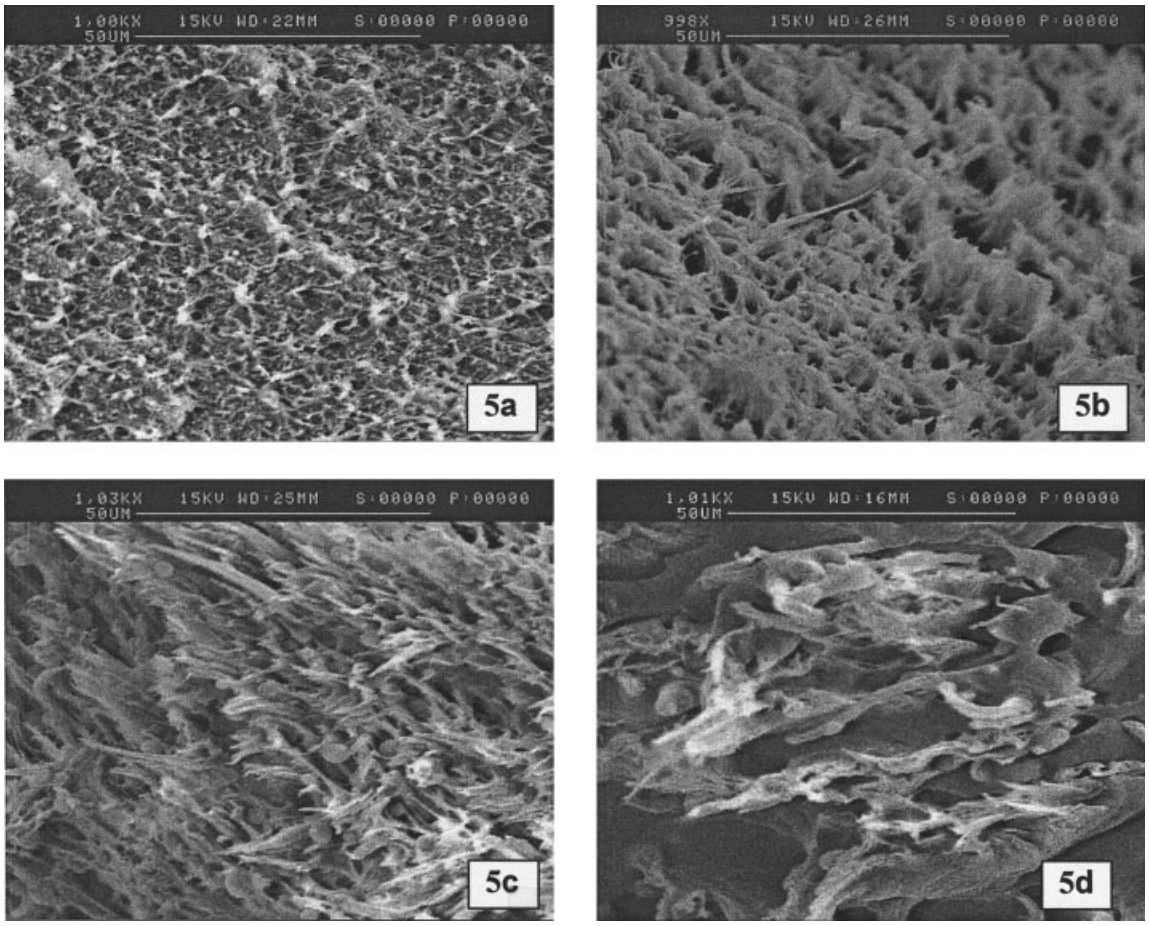

Figure 5 SEM micrographs taken of (a) control and (b–d) the tensile fractured surface of MAH-*g*-PP compatibilized PA6/PP/OMMT nanocomposites after being subjected to hygrothermal aging at (b) 30, (c) 60, and (d) 90°C.

After the PA6/PP/OMMT samples were exposed to the hot and moist environment, the OMMT reacted with water (as discussed earlier); however, the rigid, high aspect ratio and platelike structure of the OMMT remained intact. Thus, it can be anticipated that once the PA6 matrix became softened, the mismatch in thermal coefficient expansion between the polymer matrix and OMMT facilitated the formation of microcavitations in the interfacial region. The microcavitations subsequently facilitated yielding and increased the elongation at break of the PA6/PP/OMMT upon tensile deformation. Note that the direction of tensile deformation is parallel to the mold flow direction of OMMT. Furthermore, as the immersion temperature increased, the moisture attack and interaction with OMMT was faster and this may have helped to slightly increase the exfoliation/intercalation of the OMMT in the PA6/PP matrix.

Morphological study

Figure 3(a–d) shows SEM micrographs of the PA6/PP blends, highlighting the effect of immersion temperature on the morphology of PA6/PP. Irregular and large PP particles are evident. Poor interaction between PP and PA6 is indicated by the "gap" between them. The PA6/PP blend hygrothermally aged at 90°C had more brittle morphology [Fig. 3(d)]. This is in agreement with a reduction of about 50% in the elongation at break values of the PA6/PP (Table III).

Figure 4(a–d) shows the SEM micrographs of uncompatibilized PA6/PP/OMMT after being subjected to hygrothermal aging at 30, 60, and 90°C, respectively. Interestingly, the morphology of the fractured surface for the PA6/PP/OMMT has been progressively transformed from brittle failure [Fig. 4(b)] to relatively ductile behavior [Fig. 4(d)]. These observations provide good supportive evidence for the slight increment of the elongation at break displayed by the hygrothermally aged composites. Fibrillated morphology and PP particle detachment can be observed on the fractured plane. As stated earlier, water molecules can penetrate and intercalate into the gallery of the layered silicate of OMMT (exfoliated silicate layers) in the PA6 matrix. Note that, as the immersion temper-

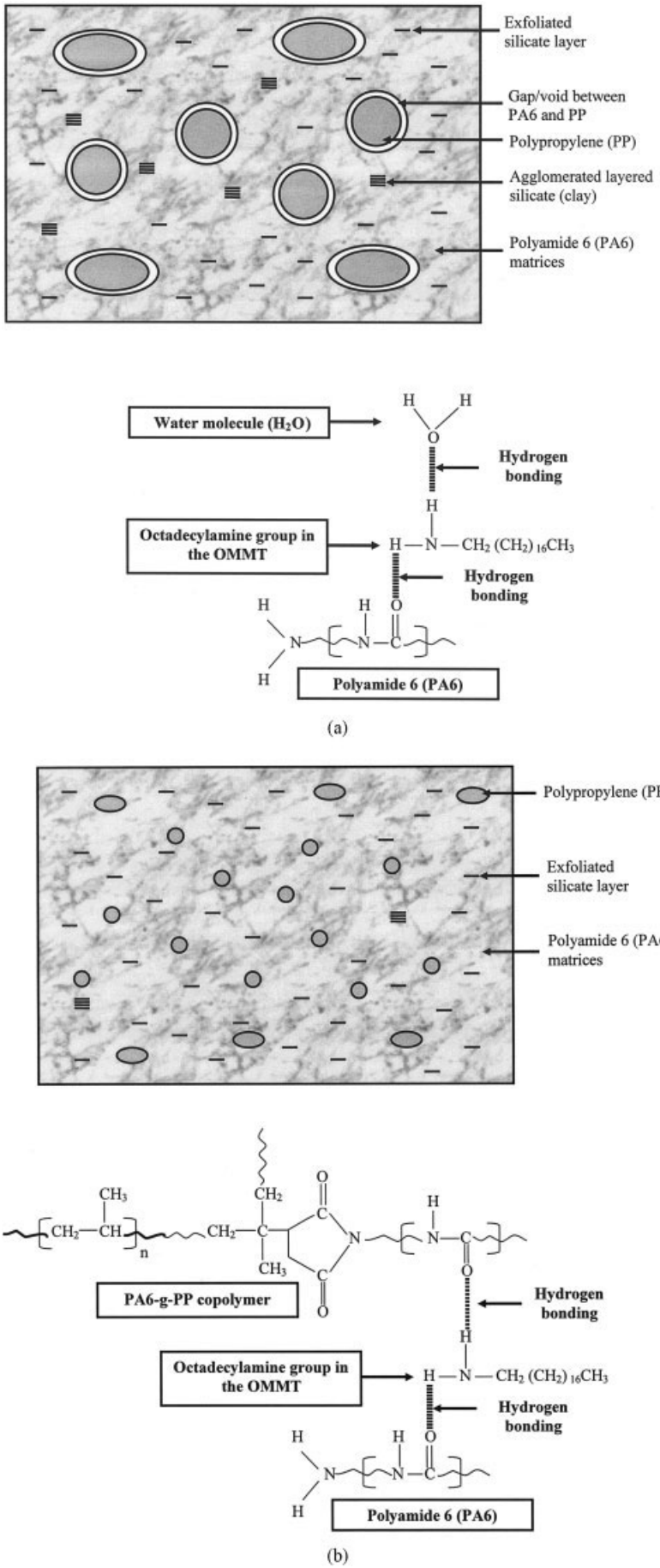

Figure 6 The proposed mechanism between the intercalant of OMMT (in the PA6 matrix) and (a) a water molecule (b) and PA6-*g*-PP. (Note the free site for H bonding with H_2O is unavailable.)

ature increases, the kinetic energy increases and the water molecules move faster, resulting in an increase of the diffusion rate (Table II). We believe that some of the water may be "entrapped" in the exfoliated silicate layer or, in other words, the water acts as a plasticizer in the OMMT interlayer gallery and consequently increases the elongation at break of the composites.

Figure 5(a–d) shows the SEM micrographs of MAH-*g*-PP compatibilized PA6/PP/OMMT nanocomposites upon being subjected to hygrothermal aging at 30, 60, and 90°C. The fibrillated morphology in the MAH-*g*-PP compatibilized PA6/PP/OMMT nanocomposites is due to the increased interfacial bonding of PA6 and PP in the presence of MAH-*g*-PP and is explained by the increase of the elongation at break of the compatibilized composites (Table II). It is interesting to note that the fibrillated morphology could still be observed even after the composite samples were subjected to hygrothermal aging at high temperature. This again provides a good indication that the exfoliation/intercalation of the OMMT in the PA6/PP matrices may be slightly increased by the combination of water and heat effects (viz., hygrothemal effect). Water may act as a plasticizer for both the PA6 matrix and the partially exfoliated/intercalated silicate layer of OMMT.

Proposed mechanism of water interaction

A possible mechanism of water interaction with PA6/PP/OMMT is proposed. Figure 6(a) shows a schematic representation of the morphology of the PA6/PP nanocomposite containing OMMT. It can be expected that the water molecules plasticize the PA6 chain in the PA6/PP matrix and interact with the octadecylamine (intercalant of OMMT), under the condition by which the layered silicate of OMMT has been exfoliated/intercalated. Thus, possible sites for water molecules interaction are available [Fig. 6(a)]. Accordingly, this explains the reason why the M_m values increase with the incorporation of OMMT (Table II). For comparison, a schematic representation of the morphology of the MAH-*g*-PP compatibilized PA6/PP/OMMT is also proposed [Fig. 6(b)]. Note that the particle size of the PP droplets is smaller, because of the compatibilization effect in the presence of MAH-*g*-PP. Recall that the OMMT was preferentially dispersed in PA6-rich and PA6-*g*-PP phases.[17] Amine groups in the OMMT may react with amide groups of PA6 and PA6-*g*-PP copolymer via hydrogen bonding. Thus, there is less possibility for the water molecules to interact with the octadecylamine, which is attributed to possible sites for bonding of the octadecylamine already being occupied by either PA6 (amide group) and MAH-*g*-PP (anhydride group). In other words, the "free" functional groups of octadecylamine in OMMT, and amide groups in PA6, are less available for water interaction. Thus, the water uptake of the MAH-*g*-PP compatibilized PA6/PP/OMMT is less compared to the uncompatibilized one, and even lower than for PA6/PP (Table II).

CONCLUSIONS

Based on this work, which was devoted to study the effect of water absorption and hygrothermal aging behavior on the mechanical and morphological properties of PA6/PP/OMMT nanocomposites, the following conclusions can be drawn:

1. The kinetics of water absorption of the PA6/PP nanocomposites conforms to Fickian law behavior. The M_m and D are dependent on the OMMT loading, MAH-*g*-PP concentration, and immersion temperatures.
2. Both the tensile modulus and strength of PA6/PP nanocomposites deteriorated after being exposed to hygrothermal aging. However, the recovery in strength and stiffness of the PA6/PP/OMMT are quite excellent at the immersion temperature of 30°C. Water merely acts as a plasticizer for the PA6/PP matrix and silicate layer of OMMT.
3. At any immersion temperature, MAH-*g*-PP compatibilized PA6/PP/OMMT nanocomposites showed excellent retention ability and recovery properties. The presence of MAH-*g*-PP not only enhanced the resistance of the nanocomposites against direct water immersion but also improved the resistance of the composites against hygrothermal attack.

The authors thank the Ministry of Science, Technology and Environment, Malaysia, for an IRPA grant. A special scholarship, granted by Universiti Sains Malaysia to the first author (W.S.C.), is gratefully acknowledged. The authors also thank Professor J. Karger-Kocsis (Kaiserslautern University of Technology) and Dr. Thomann (University of Freiburg) for their valuable input and TEM measurements, respectively.

References

1. Mohd Ishak, Z. A.; Berry, J. P. J Appl Polym Sci 1994, 51, 2145.
2. Mohd Ishak, Z. A.; Ishiaku, U. S.; Karger-Kocsis, J. J Appl Polym Sci 1999, 74, 2470.
3. Mohd Ishak, Z. A.; Ariffin, A.; Senawi, R. Eur Polym J 2001, 37, 1635.
4. Mohd Ishak, Z. A.; Ishiaku, U. S.; Karger-Kocsis, J. Comp Sci Technol 2000, 60, 803.
5. Bárány, T.; Karger-Kocsis, J.; Czigány, T. Polym Degrad Stabil 2003, 82, 271.
6. Mohd Ishak, Z. A.; Yow, B. N.; Ng, B. L.; Khalil, H. P. S. A.; Rozman, H. D. J Appl Polym Sci 2001, 81, 742.

7. Guo, B.; Jia, D.; Fu, W.; Qiu, Q. Polym Degrad Stabil 2003, 79, 521.
8. Ivanova, K. I.; Pethrick, R. A.; Affrossman, S. J Appl Polym Sci 2001, 82, 3468.
9. Vauthier, E.; Abry, J. C.; Bailliez, T.; Chateauminois, A. Comp Sci Technol 1998, 58, 687.
10. Chateauminois, A.; Vincent, B.; Chabert, L.; Soulier, J. P. Polymer 1994, 35, 4766.
11. Bao, L.-R.; Yee, A. F.; Lee, Y.-C. Polymer 2001, 42, 7327.
12. Bao, L.-R.; Yee, A. F. Polymer 2002, 43, 3987.
13. Karbhari, V. M.; Rivera, J.; Zhang, J. J Appl Polym Sci 2002, 86, 2255.
14. Han, M.-H.; Nairn, A. J. Compos Part A Appl Sci Manufac 2003, 34, 979.
15. Yang, D. K.; Koros, W. J.; Hopfenberg, H. B.; Stannett, V. T. J Appl Polym Sci 1986, 31, 1619.
16. Chow, W. S.; Mohd Ishak, Z. A.; Ishiaku, U. S.; Karger-Kocsis, J.; Apostolov, A. A. J Appl Polym Sci 2004, 91, 175.
17. Chow, W. S.; Mohd Ishak, Z. A.; Karger-Kocsis, J.; Apostolov, A. A.; Ishiaku, U. S. Polymer 2003, 44, 7427.